Zimmermann, G., Körner, A., Burkhardt, H. (2000): Hydraulic pathways in the crystalline rock of the KTB. - Geophysical Journal International, 142, 1, pp. 4—14.

DOI: http://doi.org/10.1046/j.1365-246x.2000.00119.x

Geophys. J. Int. (2000) **142,** 4–14

Hydraulic pathways in the crystalline rock of the KTB

Günter Zimmermann,[1] Alexander Körner[2] and Hans Burkhardt[1]

[1] *Institüt Angewandte Geophysik, Technische Universität Berlin, Ackerstrasse* 76, D-13355 *Berlin, Germany. E-mail: zimm1638@geoph035.bg.tu-berlin.de*

[2] *GeoForschungsZentrum Potsdam, Telegrafenberg,* D-14473 *Potsdam, Germany. E-mail: koern@gfz-potsdam.de*

Accepted 2000 January 3. Received 1999 December 20; in original form 1999 January 12

SUMMARY

Fracture systems and fluid pathways must be analysed in order to understand the dynamical processes in the upper crust. Various deterministic as well as stochastic fracture networks in the depth section of the Franconian Lineament (6900 to 7140 m), which appears as a brittle ductile shear zone and prominent seismic reflector, were modelled to simulate the hydraulic situation at the two boreholes of the Continental Deep Drilling Program (KTB). They led to estimations of the hydraulic permeability in crystalline rock. The geometrical parameters of the fractures, such as fracture locations and orientations, were determined from structural borehole measurements, which create an image of the borehole wall. The selection of potentially open fractures was decided according to the stress field. Only fractures with the dip direction (azimuth) of the fracture plane perpendicular to the maximum horizontal stress field were assumed to be open. The motivation for this assumption is the fact that the maximum horizontal stress is higher than the vertical stress from the formation, indicating that the state of stress is a strike-slip faulting. Therefore, the probability of open fractures due to this particular stress field at the KTB sites is enhanced.

Length scales for fracture apertures and extensions were stochastically varied and calibrated by hydraulic experiments. The mean fracture aperture was estimated to be 25 μm, assuming an exponential distribution, with corresponding permeability in the range of 10^{-16} m^2. Similar results were also obtained for log-normal and normal distributions, with a variation of permeability of the order of a factor of 2. The influence of the fracture length on permeability of the stochastic networks was also studied. Decreasing the fracture length beyond a specific threshold of 10 m led to networks with vanishing connectivity and hence vanishing permeability. Therefore, we assume a mean fracture length exceeding the threshold of 10 m as a necessary assumption for a macroscopic hydraulically active fracture system at the KTB site. The calculated porosity due to the fracture network is of the order of 10^{-3} per cent, which at first sight contradicts the estimated matrix porosity of 1 to 2 per cent from borehole measurements and core measurements. It can be concluded from these results, however, that if the fluid transport is due to a macroscopic fracture system, only very low porosity is needed for hydraulic flow with permeabilities up to several 10^{-16} m^2, and hence the contribution of matrix porosity to the hydraulic transport is of a subordinate nature.

Key words: borehole geophysics, fluid dynamics, fractures, permeability.

INTRODUCTION

The KTB site is located in the Variscan basement at the northwestern margin of the Bohemian Massif. The Franconian lineament separates the South German sedimentary basin from the crystalline rocks of the Bohemian Massif. This NW–SE-trending fault system, dipping approximately 50°–55° NE underneath the basement (Harjes *et al.* 1997), strikes the KTB main borehole in the depth range of 7000 m (Wagner *et al.* 1997). The Franconian lineament appears as a brittle ductile shear zone with open fractures and fault planes perpendicular to the minimum horizontal principal stress (Brudy *et al.* 1997).

The porosity and permeability of rock are strongly dependent on pressure and temperature. Extrapolation of these quantities measured on core samples under ambient conditions to *in situ* conditions leads to unrealistic values. The values of matrix

permeability measurements on cores from the KTB wells are in the range from 10^{-20} to 10^{-18} m^2 (Huenges *et al.* 1997), but one has to take into account that cores only cover intergranular and not macroscopic pathways such as open faults and fractures. Formation porosity was measured on cores and estimated from borehole measurements and is in the range of 1 per cent (Zimmermann *et al.* 1992; Pechnig *et al.* 1997).

In situ permeability can be determined by hydraulic tests. Various kinds of tests can be carried out, depending on transmissivity and location. Tests in the open hole cover the whole borehole except for the parts isolated hydraulically due to casing and cementation. The resulting transmissivities therefore represent mean values for the whole interval and can differ significantly from isolated inflow horizons. Locally limited intervals can be investigated with packer tests. Several hydraulic tests were carried out in KTB-VB (the pilot hole) and KTB-HB (the deep hole) to determine the *in situ* permeability (Huenges *et al.* 1997). These tests yielded permeability values in the range from 10^{-17} to 5×10^{-16} m^2; a clear depth dependence cannot be detected. The discrepancy between the mean values of the core measurements ($\sim 10^{-19}$ m^2) and the hydraulic results is about three orders of magnitude. This is interpreted as a scale dependence of permeability (Brace 1984; Clauser 1992); that is, permeability measurements give different results depending on the scale of the volume under investigation. Injection tests between 6000 and 8700 m yielded permeability values in the range of the core measurements; this is due to the low size of the test volume and the infiltration of mud into the rock, leading to sealing of the rock.

Therefore, small matrix permeability and relatively high macroscopic permeability give hints of the existence of a macroscopic network of open fractures (Kessels & Kück 1995). A first possibility to estimate the lateral extent of a fracture network is the formation pressure. At the final depth of the main borehole (9101 m) the formation pressure was determined to be 103 MPa (Huenges *et al.* 1997), equivalent to a hydrostatic water head with respect to increasing density due to (increasing) salinity. This points to a network of possible pathways of several kilometres in the vertical direction, where fluids are not exposed to lithostatic pressure. Other indications for a considerable extent of the fracture system are visible in the communication experiments between the wells. Measurements of the fluid level in the pilot well during draw-down tests in the main borehole in the depth interval from 3000 to 6000 m and at the final depth of 9101 m show a drop in the mud level. These results suggest pathways for fluids between the boreholes with a horizontal distance of 200 m and a vertical distance of more than 4000 m.

MODELLING FRACTURE PERMEABILITY: THE DIFFERENT STEPS

The aim of this work is the geometrical identification of hydraulically active fractures in the depth section of the Franconian Lineament (6900 to 7140 m), construction of discrete deterministic as well as stochastic fracture networks from these geometrical data, and subsequent calculation of permeability from these networks. Fluid flow is simulated by applying Darcy's law (Guéguen & Palciauskas 1994) assuming fluid velocities with laminar flow. A simple description of a fracture can be given by a smooth fracture plane, neglecting effects like roughness. Generally, fracture planes can be described by the length and width of the fracture plane (surface area), the fracture thickness or aperture, and the orientation (dip, azimuth) of the fracture. Using a projection area, this description of a 3-D fracture plane can be reduced to a 2-D problem, and the geometry description of the surface area is reduced to a fracture length and spacing.

Reduction to a 2-D problem deserves some additional explanation of the assumptions that are made. First of all, if a 3-D network is reduced to a 2-D network, the resulting 2-D network must remain a connected network. This can be achieved if the projection area is set to be approximately perpendicular to the preferred orientation of the fracture planes; in this case, optimal intersections between the fractures are obtained. This procedure fails if the 3-D network is connected but all 2-D projections are not. This is the point where the 2-D connectivity drops below the percolation threshold. As long as we expect a 2-D percolation probability above the percolation threshold, a description of a 3-D network by a 2-D projection area is an acceptable simplification, with the advantage that there is one less unknown parameter to determine, namely the fracture extension in the third dimension.

The problem is highly underdetermined. Therefore, besides the known basic information about the fractures, additional data and calibrations are needed to give a well-constrained estimate of permeability and to allow a discussion of the limitations of unknown quantities and their influence on permeability in the geometric networks. The procedure is as follows. First, the geometry of fracture planes, such as dip, azimuth and depth, is determined by so-called structural borehole measurements, which produce an image of resistivity contrasts of the borehole wall. Second, the origins of the structures have to be ascertained, and open fractures have to be extracted from the data set. Generally, the conductive structures identified can be of electronic or electrolytic origin or a mixture of both. Therefore, a clear distinction between fracture structures of electrolytic origin (saline fluids) and other conductive structures (graphite or ore minerals) is not possible from this primary information. For this reason, we use additional information about the stress field as a criterion to distinguish between potentially open and closed fractures. Using the above criteria, a data set of geometrical information on potentially open fractures can be obtained to serve as input for hydraulic networks.

Additional information is necessary to determine the fracture aperture, the fracture lengths, and the corresponding distribution functions. Owing to the fact that a linear change of fracture aperture results in a change of permeability according to the 'cubic law' (Priest 1993), this parameter plays a crucial role in fracture permeability. In addition, the fracture length is also a critical parameter, since it controls the connectivity. We investigate this case by constructing several networks with different but constant fracture lengths to study the influence on permeability. A more general approach is given by Gavrilenko & Guéguen (1998), who introduced a modified renormalization method with multiscale networks and broad distribution functions for hydraulic conductances and fracture lengths.

STRUCTURE IDENTIFICATION AND SELECTION OF OPEN FRACTURES

The geometrical structure of the fractures can be determined by the structural borehole logs, giving an image of the

borehole wall. The Formation Micro Imager (FMI) and the Hostile Environment Logging (HEL) Formation Micro Scanner (HFMS) are logging tools which create a microresistivity image. These tools consist of four arms with one (HFMS) or two pads (FMI) with rows of small electrodes to determine the resistivity image of the borehole wall on a microscopic scale [distance between the electrodes is 7.62 mm (HFMS) or 5.08 mm (FMI)]. The coverage of the tools depends on the borehole diameter. For the HFMS, which was used below 6000 m because of the higher temperature (>175 °C), the coverage was 25 per cent at a caliper of 12.25 inches (Fig. 1). The geometrical orientation of the fractures (dip, azimuth, depth) can be determined by interactively picking the images of the fractures with a computer program.

The electrical conductivity contrast seen in the FMS measurements has a twofold origin, which complicates the selection of open fractures. The localized structures can be foliation planes containing graphite, as well as recrystallized and potentially open and fluid-bearing fractures. Therefore, we have to distinguish between these structures to identify the open fractures. Secondary minerals in the cataclastic shear and fault zones contain graphite in proportions of up to 10 per cent, which appears to be a recrystallization product from fluids (Möller *et al.* 1997), and iron sulphides, belonging to the Upper Carboniferous reverse faulting event (ELEKTB 1997). These minerals possess a high electrical conductivity which is measured by FMS, but are mainly restricted to the paragneiss sections. The ELEKTB group investigated polished sections from cuttings and assumed an electronic origin of electrical conductivity if the cuttings show an increased content of graphite and sulphide. By comparison with laterolog measurements, they stated that 73 per cent of all resistivity minima measured

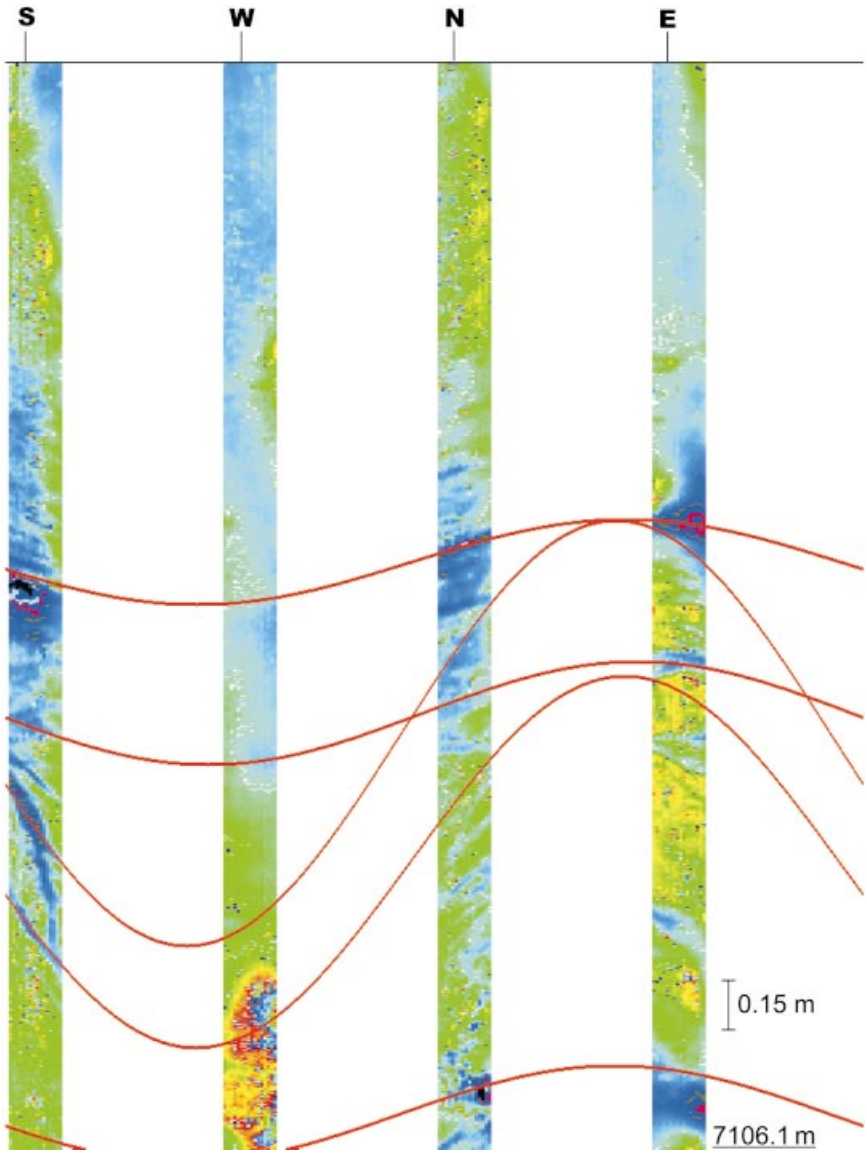

Figure 1. Image of the Hostile Environment Logging (HEL) Formation Micro Scanner (HFMS) in the depth range from 7103 m to 7106 m of the KTB-HB. This logging tool creates a microresistivity image of the borehole wall. Geometrical parameters such as depth, dip and azimuth of the striking fractures can be picked interactively. The scale of electrical resistivity passes from dark blue (low) through green/yellow (mid) to red (high) colours. Fractures appear as dark blue structures. Five fractures are marked and occur as sinusoidal functions. The coverage of the tool is approximately 25 per cent of the borehole wall.

by the laterolog are controlled by electronic conduction of graphite and ore minerals, while 27 per cent are due to electrolytic conduction from saline fluids. However, it is not the presence of graphite and saline fluids that produces the resistivity minima in the laterolog measurements. The controlling factor is the connectivity (ELEKTB 1997).

Generally, the distinction between foliation planes and fractures by FMS measurements without further information is difficult, and it is impossible to distinguish between open and closed fractures by FMS measurements alone. Nevertheless, a fracture log can be determined from these measurements which can be used as a first indication for the frequency and geometry of potentially hydraulic conductive structures. To distinguish between open and closed fractures the orientation of the stress field is used and an additional assumption is introduced.

The direction and the magnitude of the *in situ* principal stresses in the KTB boreholes were determined by combined analysis of breakout orientation and of drilling-induced tensile fractures (Brudy *et al.* 1997). Breakouts and drilling-induced fractures are a reaction of the formation to the borehole. The stress condition is disturbed and leads to breakouts due to relaxation in the direction of the minimum horizontal stress. Drilling-induced fractures occur perpendicular to the breakouts and are therefore in the direction of the maximum horizontal stress. From these data the orientation of the maximum horizontal stress as a function of depth was determined by Brudy *et al.* (1997).

A hydrofrac experiment carried out in the depth range of 6018 m in KTB-HB led to the determination of the least horizontal stress as $\sigma_h = 110$ MPa. The upper and lower bounds of the maximum and minimum horizontal stress were estimated by Brudy *et al.* (1997); the vertical stress σ_v can be calculated from the vertical thickness z and the mean rock density ρ:

$$\sigma_H = 250\text{–}330 \text{ MPa}\,(\text{N}164^\circ); \quad \sigma_h = 130\text{–}160 \text{ MPa}\,(\text{N}74^\circ);$$

$$\sigma_v = \rho g z = 192 \text{ MPa}, \text{ with } \rho = 2.8 \text{ g cm}^{-3},$$

$$g = 9.81 \text{ m s}^{-2}, \quad z = 7.0 \text{ km}.$$

This result shows that the vertical stress from the formation in the depth interval of the Franconian lineament is the intermediate stress ($\sigma_H > \sigma_v > \sigma_h$), indicating that the present state of stress is strike-slip faulting (Zoback & Harjes 1997).

The Franconian Lineament, which appears as a NW–SE-trending surface boundary between the Variscan basement and the Permo-Mesozoic sedimentary basins, was probably formed in the Late Palaeozoic and was reactivated as a reverse fault in the Mesozoic (Wagner *et al.* 1997). Wagner *et al.* showed from overprinting relations that faults and veins can be separated into late Variscan and post-Variscan structures, with late Variscan deformation resulting in subvertical extensional veins and brittle–ductile reverse faults, and post-Variscan structures occurring as subhorizontal extensional veins and brittle reverse and normal faults.

The decoupling of the fluid pressure from lithostatic pressure is only possible for fracture systems that remain open, as a result of the stress state, and have a vertical extension of up to a few kilometres, so that hydraulic communication between the formation fluids can be maintained (Huenges *et al.* 1997). The steeply inclined reverse faults and fractures, which are the youngest deformation structures, can be kept open over a long period of time under the present stress regime and are responsible for a hydraulically active fracture system.

As a result of these conditions, fractures are assumed to be open fractures if the following criteria are fulfilled:

(1) the azimuth of the fracture plane (the dip direction) is perpendicular to the maximum horizontal stress field σ_H;
(2) the fractures are steeply dipping with dip angles similar to that of the SE1 reflector (50°–55°).

The first condition is the most important and necessary one; the second condition can be considered as an addition, which is nearly always fulfilled at the KTB with its steeply dipping formation. Therefore, this is equivalent to the fact that the fracture plane is nearly perpendicular to the minimum horizontal stress σ_h (see Fig. 2).

We admit a deviation of up to $\pm 20^\circ$ from the preferred orientation. This is because we examined high resistivity contrasts in the FMS measurements for fractures with this

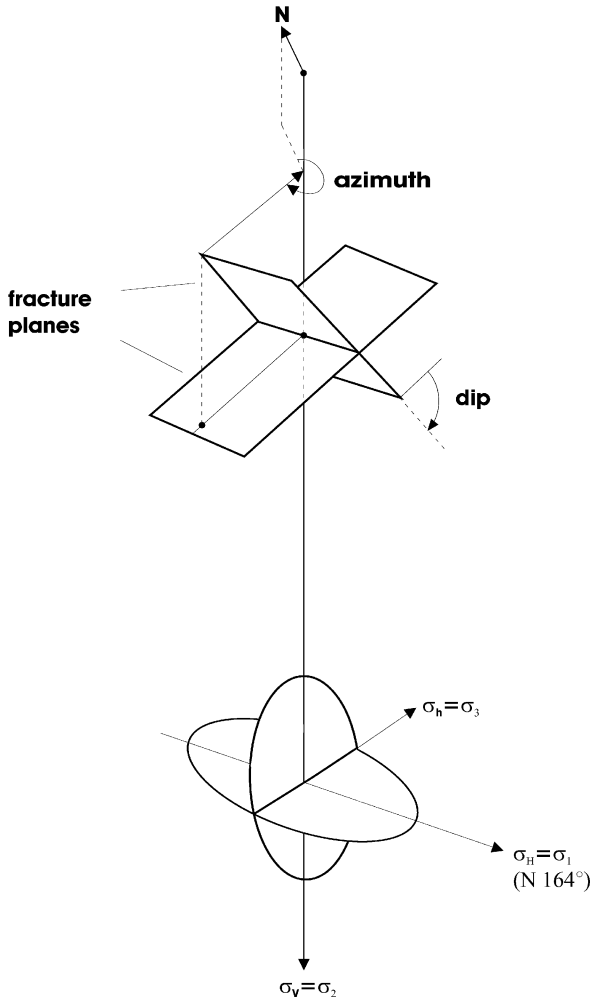

Figure 2. Observed fracture planes from reverse faulting and the present stress ellipsoid. The maximum horizontal stress is in the direction N164° (after Brudy *et al.* 1997) and the vertical stress is the intermediate stress, indicating that the state of stress is a strike-slip faulting (Zoback & Harjes 1997). Therefore, we assume that fracture planes with an azimuth perpendicular to the maximum horizontal stress and a steeply dipping angle are potentially open.

preferred orientation, which supports the selection according to the stress criteria. Therefore, we assume the fractures to be open if the azimuth (the dip direction) is orientated perpendicular to the maximum horizontal stress field with a deviation of 20°. Admitting only positive dip angles, this results in two data sets with an azimuth difference of 180°. The second stress criterion of steeply dipping angles is automatically fulfilled for all fractures.

For the depth interval of the Franconian lineament (6900 to 7140 m), a total of 312 fractures were detected by FMS, but only 67 fractures passed the stress criterion. Finally, two data sets of potentially open fractures were obtained, with mean azimuths of N75° and N255°, respectively, and steep dipping angles with a mean value of 55°.

The two sets of fractures that have been selected have being checked against FMS measurements. They show the highest conductivity contrast in the FMS measurements. Therefore, the selection of open fractures due to the stress field is supported by the FMS measurements, even if the conductivity contrast is not a definite indication by itself.

DETERMINATION OF THE LINEAR FREQUENCY OF FRACTURES

The two data sets from the Franconian Lineament were used to determine the linear fracture frequency, λ_L, which is the reciprocal of the mean spacing between the fractures. This is defined as the quotient of the number of fractures N_{Fr} in a given depth interval and its length L:

$$\lambda_L = N_{Fr}/L. \quad (1)$$

If the linear fracture frequency refers to the whole population of the fractures, it is called the total linear frequency, $\lambda_{L;total}$. If it refers to one of the fracture sets, it is called the linear frequency of the set, $\lambda_{L;set}$. An additional way to define the fracture frequency is by its relation to the fracture distances (spacing) X_j. If $N_{Fr} - 1$ distances X_j between the fractures are measured, the mean spacing is defined as

$$\bar{X} := \frac{1}{(N_{Fr}-1)} \sum_{j:=1}^{(N_{Fr}-1)} X_j, \quad (2)$$

and λ_L is the reciprocal of the mean spacing.

Table 1 shows the results of the fracture frequency calculations for the total population and the two sets in the depth section of the Franconian lineament. For the total population and the two sets of fractures the only depth sections taken into consideration were those where we actually found fractures meeting the stress criterion. Therefore, the frequency for the total population is smaller than that for set 1. Because of missing data in the FMS measurements due to borehole breakouts in the depth section from 7000 to 7030 m, this gap was closed with additional artificially produced fractures. The parameters of these fractures were determined from the statistical parameters of the remaining interval and included in the data set. From the linear frequencies of the two sets the calculation yields

$$\lambda_{L;set1} = 0.296\ m^{-1} \Rightarrow 9\ \text{fractures},$$

$$\lambda_{L;set2} = 0.078\ m^{-1} \Rightarrow 3\ \text{fractures}.$$

The individual dips of the fractures were generated using the mean dip and the standard deviation of the data sets assuming a normal (Gaussian) distribution, which is determined by mean and standard deviation. The depths of the fractures were generated assuming a Poisson distribution, which describes the random occurrence of discontinuities along a line (Priest 1993).

Table 1. Comparison of the linear fracture frequencies λ_L for the two sets and the total set calculated from the number of fractures per interval and from the mean fracture spacing. Both methods lead to the same result. L_{SL} represents the scanline of the borehole interval where the fractures were detected, and N_{FR} is the number of fractures.

	total	set1	set2
N_{FR}	67	49	18
depth interval	6900 m–7135 m	6900 m–7062 m	6919 m–7136 m
L_{SL}	235 m	162 m	217 m
$\lambda_L := N_{FR}/L_{SL}$	0.284 m^{-1}	0.302 m^{-1}	0.083 m^{-1}
$\lambda_L := 1/X$	0.280 m^{-1}	0.296 m^{-1}	0.078 m^{-1}

RESULTS OF MODELLING

Estimation of fracture aperture

For a first estimate of the fracture aperture, a 3-D fracture network of the Franconian Lineament (depth interval 6900 m to 7140 m) was constructed and reduced to a projection area. As input parameters, we used the results from the FMS measurements (depth, dip and azimuth of the two fracture sets). The extensions of the fracture planes are initially unknown parameters. Therefore, for a first estimate all fractures pass through the whole model from one boundary to the other. The projection was carried out in the W–E direction along the borehole axis, leading to a 2-D fracture network. The projection plane is thus nearly perpendicular to the maximum horizontal stress (N174°), which leads to a well-connected 2-D network. The projection area of the model is 240 m by 10 m, i.e. 5 m to each side from the borehole axis (Fig. 3). The distance from the borehole axis to the border of the model was initially chosen arbitrarily, but has no influence on the permeability calculations if two conditions are fulfilled. First, the fracture planes must be of infinite extension; that is, they must connect the right and left borders of the model as mentioned above. Second, each fracture must have a constant fracture aperture. We proved these conditions analytically with a connected network, and in addition tested the finite element program ROCKFLOW, which was developed to study the hydraulic flow and transport mechanisms in fractured rock (Lege *et al.* 1996). Furthermore, we proved that the number of intersections between the fractures has no influence on the fluid transport, and hence permeability, if the two conditions are fulfilled. The situation changes significantly if the fracture aperture is varied between the nodes (the intersections) of the fractures. We discuss this situation below in detail for the stochastic networks. In this case, we have a network of hydraulic resistors, and the intersections play an important role for the network permeability, even for fractures limited only by the border of the model.

The corresponding permeability was calculated in the horizontal direction according to Darcy's law for models with different but constant fracture apertures. Table 2 shows the results of the calculated horizontal fluid flow and mean macroscopic fluid velocity assuming a pressure gradient of 10^4 Pa m^{-1},

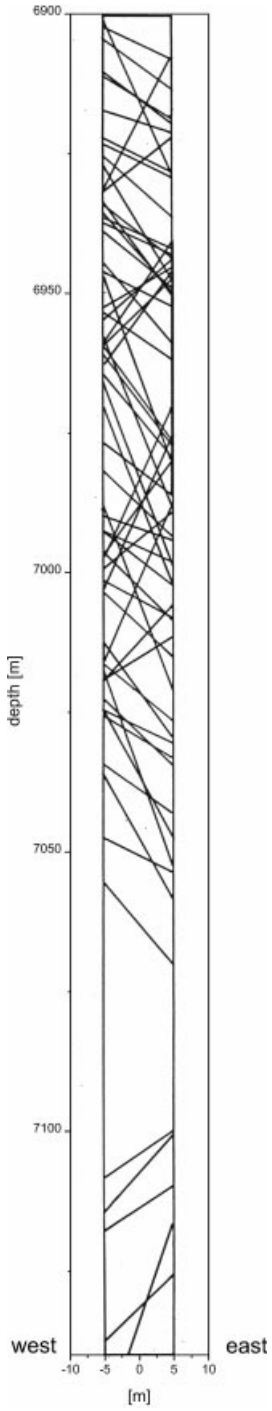

Figure 3. Fracture network in the depth section of the Franconian lineament with fracture lengths exceeding the border of the projection area of 240 m by 10 m (projection in W–E direction). The fluid flow was calculated in the horizontal direction.

and the corresponding permeability for various fracture apertures. The dependence of permeability on fracture aperture is according to the 'cubic law' (Priest 1993). Comparison of the calculated permeability with the *in situ* permeability determined by hydraulic tests of approximately 2×10^{-16} m^2 (Huenges *et al.* 1997) leads to a first estimation of the fracture aperture of approximately 25 μm.

Table 2. Permeability calculations in the horizontal direction for various fracture apertures. The depth interval is related to the vertical extension of the Franconian lineament (k^{240}_{horizon}). A fracture aperture of $a = 25$ μm reproduces the *in situ* permeability of the KTB main hole (KTB-HB). The flow volume per unit time and the macroscopic velocity of fluids in the fracture network were calculated assuming a pressure gradient of 10^4 Pa m^{-1}.

$a = \text{const}$ [μm]	Q_{horizon} [m^3 s^{-1}]	k^{240}_{horizon} [m^2]	$\lvert v_{\text{horizon}} \rvert$ [mm s^{-1}]
100	3.63×10^{-5}	15130×10^{-18}	5.0
50	4.53×10^{-6}	1890×10^{-18}	1.0
25	5.67×10^{-7}	236×10^{-18}	0.3
12.5	7.09×10^{-8}	29×10^{-18}	0.04

STOCHASTIC FRACTURE MODELS OF THE FRANCONIAN LINEAMENT

In the previous section a network was constructed that is a simplification of the real structure of rock. To obtain a more realistic view of the hydraulic behaviour, this simple model was modified to a stochastic network with finite fracture length. To construct the stochastic networks, instead of the original fracture geometry from the FMS measurements, the statistical mean and standard deviations of the azimuth and dip and randomly distributed locations (fracture frequency per unit area λ_A) are used. The linear frequency λ_L has to be converted into the fracture frequency per unit area λ_A. This quantity can be calculated from the known linear frequency λ_L assuming a mean fracture length μ_L. This quantity is unknown. Therefore, the use of 1-D data (λ_L) to build a 2-D model (λ_A) requires the introduction of a new parameter μ_L Priest (1993) gives a lower and an upper bound for the relation between λ_A and λ_L of spatially random distributed and parallel fractures:

$$\frac{2}{\pi}\lambda_A\mu_L \le \lambda_L \le \lambda_A\mu_L, \tag{3}$$

with μ_L the mean fracture length

Using the upper bound (for parallel fractures), because we have a preferred orientation rather than a random distribution, and a constant fracture length $\mu_L = l_{\text{fracture}}$, this leads to

$$\lambda_A = \lambda_L / l_{\text{fracture}}. \tag{4}$$

We tested this relation by simulation of a virtual borehole (vertical projections in the 2-D network), which gives a correct reproduction of the linear frequency.

The fracture length is an unknown quantity with regard to the basic information from the FMS measurements. Without any further information only a lower bound can be given, that of the diameter of the borehole, which is of the order of 0.5 m. At the other extreme, the hydraulic communication between the pilot hole (VB) and the deep hole (HB) (Kessels & Kück 1995; Huenges *et al.* 1997) suggests fracture connections through several fractures of the order of the distance between the boreholes (200 m in the horizontal direction). Therefore, different models with varying fracture length (100 m, 50 m, 30 m and 10 m) were constructed to study the influence of this parameter. This was realized for four different fracture lengths, with the two fracture sets representing the two main orientations. The W–E direction, which is nearly perpendicular

to the orientation of the two fracture sets, was selected as the projection plane. In this projection plane, the two sets are nearly perpendicular to each other and therefore give a well-connected network. For the distribution of the dip and azimuth of the fracture sets, the bivariate normal distribution was used. The origins of the fractures were generated assuming a 2-D Poisson distribution (Table 3), because without any further information about clustering, etc., the occurrence of discontinuities was assumed to be random and therefore governed by a Poisson process (Priest 1993). The original fracture network was 400 m by 400 m and then reduced to 200 m by 240 m to omit border effects. The reason for the border effect is that the number of fractures is reduced near the border, because the origin of the fractures is always within the network. The resulting two sets of fractures were then combined into one fracture model representing the stochastic information of the fracture log measurements. This model does not represent the original depth and geometry of the fractures (Fig. 4), but from a statistical point of view it is a hydraulically equivalent model.

The active node density of a network λ_{net} is defined as the number of hydraulically active nodes N_{hydr} in the network per unit area A:

$$\lambda_{net} = N_{hydr}/A\,. \tag{5}$$

Table 3. Stochastic parameters and distribution functions to generate four networks with different fracture lengths. All processes to generate the networks are independent and were carried out for each fracture set (σ is the standard deviation; L_{FR}^{Set} is the fracture length; N_{FR}^{Set} is the number of fractures; $A_{GEN} = 160000\ m^2$ = original projection area).

	distribution function	set1	set2
L_{FR}^{Set}	constant	100 m	100 m
N_{FR}^{Set}	poisson	523	155
mean azimuth $\pm\sigma$	normal	$75^\circ \pm 13^\circ$	$255^\circ \pm 11^\circ$
mean dip $\pm\sigma$	normal	$52^\circ \pm 16^\circ$	$55^\circ \pm 14^\circ$
L_{FR}^{Set}	constant	50 m	50 m
N_{FR}^{Set}	poisson	1046	310
mean azimuth $\pm\sigma$	normal	$75^\circ \pm 13^\circ$	$255^\circ \pm 11^\circ$
mean dip $\pm\sigma$	normal	$52^\circ \pm 16^\circ$	$55^\circ \pm 14^\circ$
L_{FR}^{Set}	constant	30 m	30 m
N_{FR}^{Set}	poisson	1744	517
mean azimuth $\pm\sigma$	normal	$75^\circ \pm 13^\circ$	$255^\circ \pm 11^\circ$
mean dip $\pm\sigma$	normal	$52^\circ \pm 16^\circ$	$55^\circ \pm 14^\circ$
L_{FR}^{Set}	constant	10 m	10 m
N_{FR}^{Set}	poisson	5232	1552
mean azimuth $\pm\sigma$	normal	$75^\circ \pm 13^\circ$	$255^\circ \pm 11^\circ$
mean dip $\pm\sigma$	normal	$52^\circ \pm 16^\circ$	$55^\circ \pm 14^\circ$

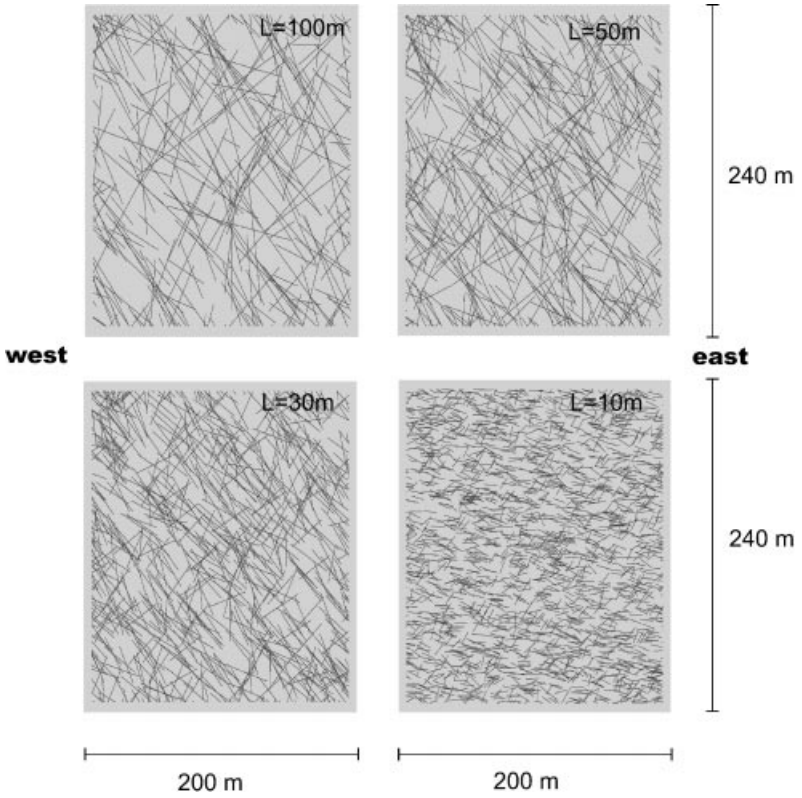

Figure 4. Stochastic fracture networks used for modelling with geometrical data from the depth section of the Franconian lineament (6900 m to 7140 m KTB-HB, projection in the W–E direction). The orientation of the fractures (the dip direction) is perpendicular to the maximum horizontal stress (N164°, Brudy *et al.* 1997) and is divided into two sets with a difference in azimuth of 180°. The number of fractures per unit area was calculated from the fractures detected from FMS measurements; the fracture length was set to 10, 30, 50 and 100 m. Variation of the mean fracture aperture leads to different permeability estimations (Table 7 and Fig. 5). The network with the fracture length of 10 m is not permeable; that is, there is no hydraulic pathway between the boundaries of the model and hence the fracture system is not connected.

Table 4. Active node density and population of the nodes for the fracture networks. All networks consist of a similar number of hydraulically active nodes (N_{hyd}) and have the same node density (~ 0.05 nodes m^{-2}). (N_{total} is the total number of nodes; N_X is the number of connected nodes in the network; $N_{boundary}$ is the number of nodes at the boundary; N_{end} is the number of nodes at dead ends; N_{fr}^{total} is the total number of fractures; N_{hyd} is the number of hydraulically active nodes; λ_{net} is the active node density; A is the projection area; and $\lambda_{fr,fr}$ is the number of intersections per fracture.).

	L100	L50	L30	L10
N_{total}	2869	3131	3932	6565
$N_X = N_{total} - N_{end}$	2205	2085	2284	2195
$N_{boundary}$	250	239	255	249
N_{end}	664	1046	1648	4370
N_{fr}^{total}	332	523	824	2185
$N_{hyd} = N_X + N_{boundary}$	2455	2324	2539	2444
$\lambda_{net} = N_{hyd}/A$	0.0511 m^{-2}	0.0484 m^{-2}	0.0529 m^{-2}	0.0509 m^{-2}
$\lambda_{fr,fr} = N_X/N_{fr}^{total}$	6.6/fracture	4.0/fracture	2.8/fracture	1.0/fracture

This density dependence of the permeability in 2-D fracture networks was first discussed by Long & Witherspoon (1985) and Hestir & Long (1990), leading to similar results as in this work, although they used different definitions to construct their networks. They generated the fractures using the active node density in contrast to this work, where the fracture frequency is the basic input.

Table 4 shows the number of nodes, the active node density and the mean number of intersections for each fracture for the four generated networks with mean fracture lengths of 10, 30, 50 and 100 m (Fig. 4).

DETERMINATION OF PERMEABILITY

Influence of the distribution functions

For a connected network, the most crucial factor controlling permeability is the fracture aperture (according to the cubic law) and the corresponding distribution function. To study its influence on permeability, calculations with different distribution functions were carried out.

The stochastic network with a fracture length of 100 m (Fig. 4) was investigated, applying different distribution functions for the fracture aperture and assuming a mean value of 25 μm according to the previous estimation. As distribution functions, the exponential, the normal (Gaussian) and the log-normal distributions were chosen. The hydraulic flow was simulated in horizontal and vertical directions to the borehole axis with the finite element program ROCKFLOW.

For the exponential distribution, the probability density function, the mean and the variance are given by

$$f(x) = \frac{1}{a}\exp(x/a); \qquad \langle x\rangle = a; \qquad \langle x^2\rangle - \langle x\rangle^2 = a^2, \tag{6}$$

with a as the mean fracture aperture. For this distribution function, only one characteristic parameter, a, is required. The normal (Gaussian) distribution is characterized by two parameters, the mean value μ and the variance σ^2:

$$\begin{aligned} &f(x) = \frac{1}{\sigma\sqrt{2\pi}}\exp\{-0.5[(x-\mu)/\sigma]^2\};\\ &\langle x\rangle = \mu;\\ &\langle x^2\rangle - \langle x\rangle^2 = \sigma^2. \end{aligned} \tag{7}$$

The same is true for the log-normal distribution:

$$\begin{aligned} &f(x) = \frac{1}{x\sigma\sqrt{2\pi}}\exp\{-0.5[(\ln x-\mu)/\sigma]^2\};\\ &\langle x\rangle = \mu_1 = \exp(\mu + 0.5\sigma^2);\\ &\langle x^2\rangle - \langle x\rangle^2 = \mu_1^2[\exp(\sigma^2) - 1]. \end{aligned} \tag{8}$$

Calculations were carried out with a mean value of 25 μm for all distribution functions, with different standard deviations of 25 μm and 12.5 μm.

For the normal distribution, an increase of the standard deviation from 12.5 μm to 25 μm leads to a permeability increase by a factor of 2, with a higher permeability for increased scattering of the fracture aperture (higher variance) around the mean value (Table 5). This effect is due to the cubic law, which favours pathways with larger fracture apertures. The opposite is true for the log-normal distribution, which is an asymmetric distribution function with a skewness to lower values. The difference is again nearly a factor 2, but with higher permeability values for the lower standard deviation.

Table 5. Comparison of permeability calculations for various distribution functions of the fracture aperture for the L100 model (fracture length 100 m).

distribution function	permeability [10^{-18} m^2] horizontal flow mean ± standard deviation	permeability [10^{-18} m^2] vertical flow mean ± standard deviation
exponential distribution mean = 25 μm	42.6 ± 2.2	72.8 ± 14.8
normal distribution mean = 25 μm standard deviation = 12.5 μm	128.0 ± 4.6	225.0 ± 13.2
normal distribution mean = 25 μm standard deviation = 25 μm	216.2 ± 7.2	344.9 ± 18.8
log-normal distribution mean = 25 μm standard deviation = 12.5 μm	107.0 ± 6.5	179.3 ± 5.6
log-normal distribution mean = 25 μm standard deviation = 25 μm	56.7 ± 4.1	99.4 ± 6.2

The exponential distribution leads to the lowest permeability values, but the results are similar to those of the log-normal distribution.

Owing to the fact that the standard deviation of the fracture aperture is initially an unknown quantity, further analysis was carried out assuming an exponential distribution with a mean fracture aperture of 25 μm. This automatically includes a standard deviation of 25 μm and leads to similar results to the log-normal distribution with equivalent mean and variance.

Influence of fracture length

To study the influence of the fracture length, the four stochastic fracture networks already introduced were used. The permeability was calculated parallel and perpendicular to the borehole axis, simulating the fluid flow with the finite element program ROCKFLOW. Two distinct calculations were made, using two distinct assumptions concerning the hydraulic fracture aperture. In the first case it was set to be constant (value of 25 μm). In the second case, we assumed an exponential distribution function with the same mean value of 25 μm.

In the first case, the permeability is quite stable (Table 6); the L100 model with 100 m fracture length and the L30 model with 30 m fracture length differ by approximately a factor 2 in permeability. The influence of the fracture length in the network, however, changes if stochastically distributed fracture apertures are used. Table 6 shows the permeability values for two models in the case of an exponential distribution function. It can be seen that the exponential distribution leads to a higher permeability in the model with long fracture lengths (L100) compared with the equivalent model with constant fracture aperture. For the model with small fracture lengths (L30), the calculation leads to a lower permeability compared with the equivalent model with constant fracture aperture. The dependence of permeability on the direction of measurement (horizontal and vertical) for all simulations is retained ($k_h < k_v$), although the quotient k_h/k_v has a large variation without any tendency. The reason for the increase of permeability in stochastic fracture networks with large fracture apertures is the influence of one individual fracture on the hydraulic behaviour of the whole network. If a number of fractures with large fracture apertures are connected to each other and additionally to the border of the network, the fluid transport is mainly concentrated on these few fractures, leading to an increasing permeability due to the so-called 'subnetwork effect' (David *et al.* 1990), where these preferential flow paths form a subnetwork and hence control the fluid transport. This influence increases if the fracture length becomes similar to the length of the network, which is the case for the deterministic network with fractures connecting the boundaries. Therefore, the lower the mean fracture length, the lower the influence of single fractures on the whole network, and the more stable the results of the simulation. For this reason the simulations for the three networks were modified. Instead of keeping the fracture aperture of each individual fracture constant and allowing only a stochastic variation for the fractures, every pathway between the nodes (intersections) of the network received an individual fracture aperture in order to reduce the influence of particular stochastic values and hence reduce the 'subnetwork effect'. Table 7 shows the result of the simulations of the flow transport for the three networks with five stochastically equivalent simulations.

The calculated permeability of the stochastic networks decreases with decreasing mean fracture length, although the fracture density is increased simultaneously to make sure that all models are equivalent considering the primary data from the borehole measurements (Fig. 5). An additional decrease of the fracture length to 10 m leads to a stochastic network that is not connected in the horizontal and vertical directions; that is, the stochastic network is below the percolation threshold and hence the permeability is zero. The hydraulic situation at the KTB site requires a macroscopic fracture connectivity, which is indicated by the communication experiments between the two boreholes (Kessels & Kück 1995; Huenges *et al.* 1997). These facts restrict the lower boundary of the mean fracture length to approximately 10 m. Assuming a hydraulic situation at the edge of the percolation threshold, the calculated stochastic network with a fracture length of 30 m seems to be the most probable of the three connected networks.

Table 6. Comparison of permeability for constant fracture aperture and for an exponential distribution of apertures. The fluctuations of permeability for the three stochastic processes document the influence of single fractures on the fluid transport (k_h is calculated in the horizontal and k_v in the vertical direction).

exponential distribution $a = 25$ μm	permeability	L100 model [10^{-18} m^2]	L30 model [10^{-18} m^2]
1.	k_h	169	18
	k_v	567	28
2.	k_h	325	24
	k_v	345	60
3.	k_h	427	11
	k_v	591	30
const. fracture aperture $a = 25$ μm	k_h	148	74
	k_v	240	108

DETERMINATION OF FRACTURE POROSITY

The fracture porosity can be calculated from the volume of the network. In 2-D networks the porosity is defined by the quotient of the flow area and the whole area of the network.

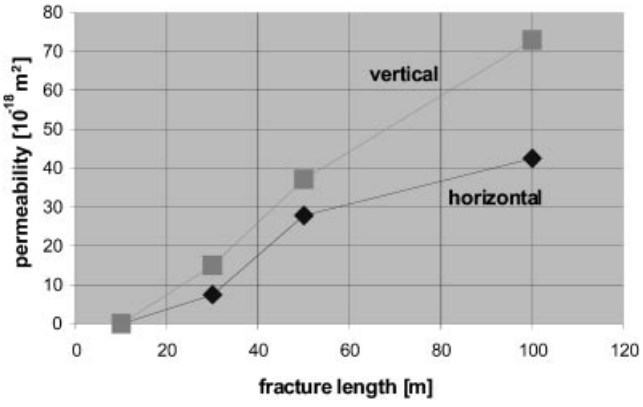

Figure 5. Permeability calculations in the horizontal and vertical directions of the stochastic networks in Fig. 4. Permeability decreases for decreasing fracture length, although the fracture density is increased simultaneously to ensure that all models are equivalent according to the primary data of the borehole measurements.

Table 7. Comparison of permeability for constant fracture aperture and for an exponential distribution of the fracture apertures between the individual nodes. The results are more stable than those in Table 6 due to the minor influence of single pathways between the nodes (k_h is calculated in the horizontal and k_v in the vertical direction).

exp. dist. $a = 25$ μm	permeability	L100 [10^{-18} m^2]	L50 [10^{-18} m^2]	L30 [10^{-18} m^2]
1.	k_h	40.0	27.0	7.8
	k_v	60.5	40.7	15.5
2.	k_h	41.4	26.2	6.9
	k_v	94.6	35.4	13.0
3.	k_h	44.0	33.0	8.3
	k_v	80.8	41.0	15.2
4.	k_h	45.6	27.2	6.3
	k_v	68.0	30.8	19.0
5.	k_h	41.9	25.5	8.2
	k_v	60.2	38.6	12.5
mean $\pm \sigma$	k_h	42.6 ± 2.2	27.8 ± 3.0	7.5 ± 0.9
	k_v	72.8 ± 14.8	37.3 ± 4.3	15.0 ± 2.6
const. fracture aperture	k_h	148	121	74
$a = 25$ μm	k_v	240	161	108

Table 8 shows the results for the three networks with constant fracture apertures. The sum of the lengths of all fractures and therefore the porosity is equal in all networks. The porosity necessary for a permeability in the range of $10^{-16} - 2 \times 10^{-16}$ m^2 is only 10^{-3} per cent. Estimations of porosity from log measurements in the KTB (Zimmermann *et al.* 1992; Pechnig *et al.* 1997) lead to values in the range of 1–2 per cent. This apparent contradiction can be explained by the concept of double formation porosity. The formation porosity is a combination of fracture porosity and matrix porosity, but only the fracture porosity makes a contribution to the fluid transport. The matrix porosity is due to microfractures, which store nearly immovable formation fluids, whereas the fluid transport is due to the network of large open fractures. Owing to these preferential hydraulic pathways, the true fluid velocities and the penetration of fluids in crystalline rock are substantially different from those in an equivalent homogeneous rock with a representative elementary volume and the same formation permeability.

Table 8. Fracture porosities ϕ_{FR} and permeabilities for the 2-D fracture networks (with constant fracture aperture) of the Franconian lineament. The contribution of the porosity of the fracture networks to the formation porosity can be neglected, but it is essential for the formation permeability. (k_h is calculated in the horizontal and k_v in the vertical direction; A is the projection area; L_{NET} is the total length of fracture network; and A_{NET} is the total network area).

	L100	L50	L30
$a = $ const.	25 μm	25 μm	25 μm
A	48000 m^2	48000 m^2	48000 m^2
L_{NET}	20020 m	20050 m	20061 m
$A_{NET} = L_{NET} \cdot a$	0.5005 m^2	0.5013 m^2	0.5015 m^2
$\phi_{FR} = A_{NET}/A$	0.001 per cent	0.001 per cent	0.001 per cent
k_h	148×10^{-18} m^2	121×10^{-18} m^2	74×10^{-18} m^2
k_v	240×10^{-18} m^2	160×10^{-18} m^2	108×10^{-18} m^2

CONCLUSIONS

A fundamental understanding of the origin, geometry and extension of the fluid pathways in crystalline rock is still incomplete. We analysed a broad spectrum of stochastic fracture networks with varying fracture apertures, fracture lengths and distribution functions in order to estimate fracture permeability at the KTB site. The problem is highly underdetermined, and therefore additional assumptions were used referring to the state of stress and the percolation threshold. Calibrations using measured permeability values from hydraulic tests were also included. Possible stochastic fracture networks and estimations of fracture apertures and fracture lengths were obtained. Under the assumptions made, these networks can describe the hydraulic situation at the KTB site.

ACKNOWLEDGMENTS

We would like to thank O. Kolditz from the Institut für Strömungsmechanik, University of Hannover for providing us with the finite element program ROCKFLOW. G. Kosakowski is acknowledged for essential help and constructive discussions. The networks were constructed using the program FracMan from Golder Associates. The authors thank the reviewers G. Müller, Y. Guéguen and H. Pape for constructive criticism and helpful comments, which greatly improved the paper. The research was financially supported by the Deutsche Forschungsgemeinschaft under grant Bu298/14.

REFERENCES

Brace, W.F., 1984. Permeability of crystalline rocks: new in situ measurements, *J. geophys. Res.,* **89,** 4327–4330.

Brudy, M., Zoback, M.D., Fuchs, K., Rummel, F. & Baumgärtner, J., 1997. Estimation of the complete stress tensor to 8 km depth in the KTB scientific drill holes: Implications for crustal strength, *J. geophys. Res.,* **102,** 18 453–18 475.

Clauser, C., 1992. Permeability of crystalline rocks, *EOS, Trans. Am. geophys. Un.,* **73,** 233–237.

David, C., Guéguen, Y. & Pampoukis, G., 1990. Effective medium theory and network theory applied to the transport properties of rock, *J. geophys. Res.,* **95,** 6993–7005.

ELEKTB Group, 1997. KTB and the electrical conductivity of the crust, *J. geophys. Res.,* **102,** 18 289–18 305.

Gavrilenko, P. & Guéguen, Y., 1998. Flow in fractured media: a modified renormalization method, *Water Resour. Res.,* **34,** 177–191.

Guéguen, Y. & Palciauskas, V., 1994. *Introduction to the Physics of Rocks,* Princeton University Press, Princeton.

Harjes, H.-P. *et al*., 1997. Origin and nature of crustal reflections: Results from integrated seismic measurements at the KTB superdeep drilling site, *J. geophys. Res.,* **102,** 18 267–18 288.

Hestir, K. & Long, J.C.S., 1990. Analyical expressions for the permeability of random two-dimensional Poisson fracture networks based on regular lattice percolation and equivalent media theories, *J. geophys. Res.,* **93,** 565–581.

Huenges, E., Erzinger, J., Kück, J., Engeser, B. & Kessels, W., 1997. The permeable crust: Geohydraulic properties down to 9101 m depth, *J. geophys. Res.,* **102,** 18 255–18 265.

Kessels, W. & Kück, J., 1995. Hydraulic communication in crystalline rocks between the two borehole of the Continental Deep Drilling Programme in Germany, *Int. J. Rock Mech. Min. Sci. Geomech.,* **32,** 37–47.

Lege, T., Kolditz, O. & Zielke, W., 1996. Strömungs- und Transportmodellierung, *Handbuch Zur Erkundung Des Untergrundes Von Deponien und Altlasten,* Springer Verlag, Berlin.

Long, J.C.S. & Witherspoon, P.A., 1985. The Relationship of the Degree of Interconnection to Permeability in Fracture Networks, *J. geophys. Res.,* **90,** 3087–3098.

Möller, P. *et al*., 1997. Paleofluids and Recent fluids in the upper continental crust: Results from the German Continental Deep Drilling Program (KTB), *J. geophys. Res.,* **102,** 18 223–18 254.

Pechnig, R., Haverkamp, S., Wohlenberg, J., Zimmermann, G. & Burkhardt, H., 1997. Integrated log interpretation in the German Continental Deep Drilling Program—Lithology, porosity, and fracture zones, *J. geophys. Res.,* **102,** 18 363–18 390.

Priest, S.D., 1993. *Discontinuity Analysis for Rock Engineering,* Chapman & Hall, London.

Wagner, G.A. *et al*., 1997. Post-Variscan thermal and tectonic evolution of the KTB site and its surroundings, *J. geophys. Res.,* **102,** 18221–18232.

Zimmermann, G., Burkhardt, H. & Melchert, M., 1992. Estimation of Porosity in Crystalline Rock by a Multivariate Statistical Approach, *Sci. Drill.,* **3,** 27–35.

Zoback, M.D. & Harjes, H.-P., 1997. Injection-induced earthquakes and crustal stress at 9 km depth at the KTB deep drilling site, Germany, *J. geophys. Res.,* **102,** 18 477–18 491.